

Weighted Encoding Based Image Interpolation With Nonlocal Linear Regression Model

Junchao Zhang

Abstract—Image interpolation is a special case of image super-resolution, where the low-resolution image is directly down-sampled from its high-resolution counterpart without blurring and noise. Therefore, assumptions adopted in super-resolution models are not valid for image interpolation. To address this problem, we propose a novel image interpolation model based on sparse representation. Two widely used priors including sparsity and nonlocal self-similarity are used as the regularization terms to enhance the stability of interpolation model. Meanwhile, we incorporate the nonlocal linear regression into this model since nonlocal similar patches could provide a better approximation to a given patch. Moreover, we propose a new approach to learn adaptive sub-dictionary online instead of clustering. For each patch, similar patches are grouped to learn adaptive sub-dictionary, generating a more sparse and accurate representation. Finally, the weighted encoding is introduced to suppress tailing of fitting residuals in data fidelity. Abundant experimental results demonstrate that our proposed method outperforms several state-of-the-art methods in terms of quantitative measures and visual quality.

Index Terms—Image interpolation, Sparse representation, Nonlocal linear regression, Nonlocal self-similarity.

I. INTRODUCTION

IMAGE interpolation is a fundamental problem in image processing, aiming to reconstruct a high resolution image from its down-sampled observation. It has wide applications in the fields of digital photography, satellite remote sensing, medical imaging and polarization imaging.

The simplest approach to reconstruct high resolution images is based on liner interpolation including Bilinear, Bicubic and Cubic-spline [1]–[3]. However, these methods estimate each missing pixel from its local neighborhood using weighted average and tend to generate artifacts in high-resolution images. To better preserve image details, more complex algorithms based on natural images priors are proposed [4]–[12]. These methods generally produce better interpolation results than liner interpolation methods. NEDI [4] is the representative edge-guided interpolation method. The local covariance coefficients from a low-resolution image are estimated firstly. Then, these coefficients are used to adapt the interpolation at high-resolution images based on the geometric duality. This method is based on the assumption of local stationarity of the covariance. However, this assumption is not completely valid and this method tends to generate artifacts in high-resolution images. The total variation model [9]–[12] is based on another prior, i.e. natural images have small first derivatives.

Sparse representation has been successfully applied in the fields of image processing and computer vision [13]–[26] and it shows promising results. For image interpolation, coupled dictionaries are jointly learned from the low- and high-resolution image patches in SCSR [17]. In this interpolation model, the low-resolution and high-resolution image patch pair share the same sparse representation with respect to their own dictionaries. Therefore, the sparse representation of a low-resolution image patch can be used to generate the corresponding high-resolution image patch. NARM [19] is another image interpolation method based on sparse representation. Nonlocal autoregressive model is embedded in NARM and nonlocal self-similarity is used as regularization term. Besides, image patches are clustered and each class is encoded by an adaptive compact dictionary. Thus, good interpolated results rely on accurate clustering. However, to cluster image patches accurately is difficulty since the class number and sample number of each class are difficulty to set. Even though experimental results in [19] showed that NARM outperforms several previous methods including SCSR, this method produces spackle noise which is generated by inappropriate clustering. A new image interpolation scheme is proposed in [23]. Non-local self-similarity assumption is adopted and over-complete dictionary is learned in this sparse model. In recent years, deep convolutional neural networks [27]–[30] provides a new strategy for image interpolation.

In this paper, we propose a new image interpolation approach based on sparse representation. Since a given pixel can be well approximated by nonlocal neighbors, we propose the nonlocal linear regression model and incorporate it into the interpolation model. Meanwhile, image sparsity prior and non-local self-similarity prior are adopted to enhance the stability of interpolation model. Current sub-dictionary learned online by clustering is difficulty since the class number and sample number of each class are difficulty to set. Inadequate clustering will reduce the accuracy of sparse representation. To address this problem, we propose a new approach to learn adaptive sub-dictionary online instead of clustering. For each patch, its non-local similar patches are grouped to train the adaptive compact dictionary, generating a more sparse and accurate representation. Moreover, since the distribution of fitting residuals is irregular than Gaussian and it has heavy tails, we introduce weighted encoding into data fidelity to suppress tailing. Abundant benchmark images are used to evaluate the interpolation performance. Experimental results demonstrate that our proposed method outperforms several state-of-the-art methods in terms of quantitative measures and visual quality.

Junchao Zhang is with School of Aeronautics and Astronautics, Central South University, Changsha 410083, China. (e-mail: junchaozhang@csu.edu.cn)

Our model is based on sparse representation, which is similar to NARM [19], but our work is unlike NARM. Our contributions can be summarized as: (1) We propose a new approach to learn adaptive sub-dictionary. For each patch, its non-local similar patches are grouped to train the adaptive compact dictionary, generating a more sparse and accurate representation. (2) We incorporate nonlocal linear regression model into interpolation model. The nonlocal linear regression model is different with autoregressive model introduced in [19]. Only weighted average is used in the autoregressive model, but our model uses weights and bias, generating a closer approximation to a given pixel. (3) We introduce weighted encoding into data fidelity to suppress tailing of fitting residuals, which ensures that the distribution of fitting residuals is more like Gaussian and the ℓ_2 norm can be still used in the data fidelity term.

The rest of the paper is organized as : the proposed interpolation model is described in Section II detailedly. Section III presents experimental results and discussions. Section IV concludes the paper.

II. WEIGHTED ENCODING WITH NONLOCAL LINEAR REGRESSION

Following the notations in [14]: for an image \mathbf{x} , $\mathbf{x}_i = \mathbf{R}_i \mathbf{x}$ denotes the i^{th} patch vector and \mathbf{R}_i denotes an extracting matrix. Given a dictionary Φ , the sparse representation of \mathbf{x}_i over dictionary Φ is: $\mathbf{x}_i = \Phi \alpha_i$, where α_i is the sparse coding coefficient with a few non-zero entries. $\|\cdot\|_0$ denotes the pseudo-norm that counts the number of non-zero entries in a vector.

A. Image interpolation with nonlocal linear regression

For image interpolation, it is assumed that a low-resolution image $\mathbf{y} \in R^M$ is directly down-sampled from its high-resolution image $\mathbf{x} \in R^N$, as formulated by Eq. (1):

$$\mathbf{y} = \mathbf{D}\mathbf{x}. \quad (1)$$

Where $\mathbf{D} \in R^{M \times N}$ is the down-sampled matrix and $N = l^2 \cdot M$ with the sampling factor l along the horizontal and vertical dimensions. According to sparse representation theory, the image interpolation problem can be transformed to minimize the following model:

$$\min_{\alpha} \left\{ \|\mathbf{y} - \mathbf{D}\Phi\alpha\|_2^2 + \lambda R(\alpha) \right\} \quad s.t. \quad \mathbf{x} = \Phi\alpha. \quad (2)$$

Where $R(\cdot)$ is the regularization term and λ is the regularization parameter. To improve the above model, we incorporate nonlocal linear regression into it. For nature images, the local linear regression model [6], [7] is used according to image local redundancy. However, the image local redundancy is inadequate to reconstruct image structures in high precision. Fortunately, nature images often have a rich amount of non-local similar patterns. These nonlocal similar patterns may be spatially either close to or far from each other. Therefore, we can establish nonlocal linear regression model using image nonlocal redundancy.

For each patch \mathbf{x}_i of size $p \times p$, we can get its similar patches in a large enough local window of size $L \times L$. A

patch \mathbf{x}_i^k is selected as a similar patch to \mathbf{x}_i if the Euclidean distance between them is not greater than the preset threshold. In fact, we can get the first m most similar patches, denoted by $\mathbf{X} = [\mathbf{x}_i^1, \mathbf{x}_i^2, \dots, \mathbf{x}_i^m]$. We define the nonlocal linear regression model between \mathbf{x}_i and \mathbf{X} as:

$$\mathbf{x}_i = \langle \mathbf{X}^T, \mathbf{a}_i \rangle + b_i. \quad (3)$$

Where \mathbf{a}_i and b_i are the weight vector and bias respectively, and $\langle \cdot \rangle$ is the inner product. We denote $\mathbf{X} = [\mathbf{x}_i^1, \mathbf{x}_i^2, \dots, \mathbf{x}_i^m, \mathbf{1}]$ and $\omega_i^T = [\mathbf{a}_i^T, b_i]$, the Eq. (3) can be rewritten as:

$$\mathbf{x}_i = \mathbf{X}\omega_i. \quad (4)$$

Because the weight vector ω_i is used to estimate the center pixel x_i of patch \mathbf{x}_i , the weight for each dimension should be different. The closer to the center pixel, the greater the weight. Here we give a simple kernel function to determine the weight as:

$$\kappa(x_i, x_j) = \exp\left(-\frac{\|d(x_i, x_j)\|_2^2}{\sigma^2}\right). \quad (5)$$

Where x_j represents neighbor pixels in a window of $p \times p$ and $d(x_i, x_j)$ represents the distance between x_i and x_j . Thus, the weight vector ω_i can be determined by solving the following regularized minimization problem:

$$\hat{\omega}_i = \arg \min_{\omega_i} \left\{ \left\| \kappa^{1/2} (\mathbf{x}_i - \mathbf{X}\omega_i) \right\|_2^2 + \chi \|\omega_i\|_2^2 \right\}. \quad (6)$$

where $\kappa = \text{diag}(\kappa(x_i, x_j))$, χ is the regularization parameter and used to avoid overfitting. The solution of Eq. (6) can be obtained by setting the derivative to zero.

$$\hat{\omega}_i = (\mathbf{X}^T \kappa \mathbf{X} + \chi \mathbf{I})^{-1} \mathbf{X}^T \kappa \mathbf{x}_i. \quad (7)$$

Then, we can get the representation of nonlocal linear regression model with $h_{i,j} = \omega_i^j$:

$$\mathbf{x} = \mathbf{H}\mathbf{x} + \mathbf{e}. \quad (8)$$

Where \mathbf{e} is the modeling error. We incorporate the above model into image interpolation model, the Eq. (2) can be rewritten as:

$$\min_{\alpha} \left\{ \|\mathbf{y} - \mathbf{D}\mathbf{H}\Phi\alpha\|_2^2 + \lambda R(\alpha) \right\} \quad s.t. \quad \mathbf{y} = \mathbf{D}\Phi\alpha. \quad (9)$$

B. Regularization terms

To solve the model formulated in Eq. (9), two widely used priors including image sparsity and non-local self-similarity are used as the regularization terms. The sparsity of coding coefficient α_i can be characterized by $\|\alpha_i\|_0$ [14], [15], [31], [32]. Non-local self-similarity prior refers to the fact that a local image patch often has many non-local similar patches to it across the image for natural images. These non-local similar patches may be spatially either close to or far from this patch. This prior has been successfully adopted in various applications of image restoration [19], [20], [22], [33]–[35].

For each patch \mathbf{x}_i of size $p \times p$, we can get its first t most similar patches by calculating the Euclidean distance between them. After we get the similar patches, denoted by $\{\mathbf{x}_i^1, \mathbf{x}_i^2, \dots, \mathbf{x}_i^t\}$, these similar patches can be used to estimate

\mathbf{x}_i by weighted average: $\hat{\mathbf{x}}_i = \sum_{k=1}^t a_k \mathbf{x}_i^k$. Term a_k is the weighted coefficient which is inversely proportional to the distance: $a_k = \exp(-\|\mathbf{x}_i - \mathbf{x}_i^k\|_2^2/h_1)/h_2$, where h_1 is a preset scalar and h_2 is a normalization factor. For a given dictionary Φ_i , we can get the sparse representations of patch \mathbf{x}_i and prediction $\hat{\mathbf{x}}_i$, i.e. $\mathbf{x}_i = \Phi_i \alpha_i$ and $\hat{\mathbf{x}}_i = \Phi_i \beta_i$. This two sparse representations should be as close as possible. In other words, the difference between α_i and β_i should be as smaller as possible. Then, image sparsity prior $\sum_i \|\alpha_i\|_0$ and nonlocal self-similarity prior $\sum_i \|\alpha_i - \beta_i\|_2^2$ are integrated into the above model. The interpolation model can be described as following:

$$\min_{\alpha} \left\{ \|\mathbf{y} - \mathbf{D}\mathbf{H}\Phi\alpha\|_2^2 + \lambda \sum_{i=1}^K \|\alpha_i\|_0 + \eta \sum_{i=1}^K \|\alpha_i - \beta_i\|_2^2 \right\} \quad s.t. \quad \mathbf{y} = \mathbf{D}\Phi\alpha. \quad (10)$$

Where K is the patch number partitioned from the image \mathbf{x} and η is the regularization parameter. Since the reweighted ℓ_p norm can enhance the sparsity and get a better solution [36], the reweighted strategy is integrated into the above model:

$$\min_{\alpha} \left\{ \|\mathbf{y} - \mathbf{D}\mathbf{H}\Phi\alpha\|_2^2 + \lambda \sum_{i=1}^K \|\alpha_i\|_0 + \sum_{i=1}^K \sum_{j=1}^{p^2} \eta_{i,j} (\alpha_{i,j} - \beta_{i,j})^2 \right\} \quad s.t. \quad \mathbf{y} = \mathbf{D}\Phi\alpha. \quad (11)$$

Where $\alpha_{i,j}, \beta_{i,j}$ are the j^{th} element of vectors α_i and β_i respectively.

C. Adaptive dictionary selection

The selection of dictionary plays an important role in the reconstruction of a signal. Lots of researches have shown to learn a universal and over-complete dictionary [14]–[17]. However, this dictionary is not effective and optimal because many atoms are irrelevant to a given local patch. Adaptive sub-dictionaries are adopted in [18]–[21]. There are two methods to train sub-dictionaries: pre-trained and online trained. Abundant high-quality images are needed for pre-trained dictionaries. However, pre-trained dictionaries are not always valid if they are irrelevant to the content of a given patch. Online trained sub-dictionaries in [19] refers to that image patches are clustered and a PCA sub-dictionary is trained for each class. However, the class number and sample number of each class are difficulty to set. Inadequate clustering will reduce the accuracy of sparse representation, leading to the inaccuracy of reconstructed signals.

In this paper, we propose a new sub-dictionary trained method. As described in non-local self-similarity priors, for each patch \mathbf{x}_i , we can get its similarity patches in a large enough local window. A patch \mathbf{x}_i^k is selected as a similar patch to \mathbf{x}_i if the Euclidean distance between them is not greater than the preset threshold. All similar patches are sorted by the Euclidean distance in ascending order. We choose the first n patches as training samples to train a PCA sub-dictionary. The term n should be large enough to guarantee a reasonable training.

These training samples are denoted as $\mathbf{x}_i^0, \mathbf{x}_i^1, \mathbf{x}_i^2, \dots, \mathbf{x}_i^{n-1}$. They are grouped as a matrix $\mathbf{X}_i = [\mathbf{x}_i^0, \mathbf{x}_i^1, \mathbf{x}_i^2, \dots, \mathbf{x}_i^{n-1}]$. Next we calculate the covariance matrix of \mathbf{X}_i , denoted by $\mathbf{C}_{\mathbf{X}_i}$. Finally we can get the adaptive PCA sub-dictionary Φ_i of the patch \mathbf{x}_i by calculating the eigenvalue decomposition of $\mathbf{C}_{\mathbf{X}_i}$:

$$\Phi_i = \mathbf{Q}^T. \quad (12)$$

Where \mathbf{Q} is the eigenvector matrix and $\mathbf{C}_{\mathbf{X}_i} = \mathbf{Q}\Sigma\mathbf{Q}^T$. In fact, these adaptive PCA sub-dictionaries form an over-complete dictionary $\Phi = [\Phi_1, \Phi_2, \Phi_3, \dots, \Phi_K]$ for image \mathbf{x} . For a given patch \mathbf{x}_i , the adaptive dictionary Φ_i is selected to code \mathbf{x}_i . This makes the sparse coding coefficient of \mathbf{x}_i over the rest sub-dictionaries be zero, leading to a very sparse representation of \mathbf{x}_i . So our method will ensure the sparsity of coding coefficient and the sparse regularization term can be removed. Thus, over adaptive sub-dictionaries, the image interpolation model can be described as:

$$\hat{\alpha} = \arg \min_{\alpha} \left\{ \|\mathbf{y} - \mathbf{D}\mathbf{H}\mathbf{x}\|_2^2 + \gamma \sum_{i=1}^K \|\mathbf{R}_i \mathbf{x} - \Phi_i \alpha_i\|_2^2 + \sum_{i=1}^K \sum_{j=1}^{p^2} \eta_{i,j} (\alpha_{i,j} - \beta_{i,j})^2 \right\} \quad s.t. \quad \mathbf{y} = \mathbf{D}\mathbf{x}. \quad (13)$$

D. Weighted encoding

Here we discuss the ℓ_2 norm data fidelity term $\|\mathbf{y} - \mathbf{D}\mathbf{H}\mathbf{x}\|_2^2$ in order to get a better solution of Eq. (13). Since the ℓ_2 norm is optimal for Gaussian distribution, a non-Gaussian distribution of fitting residuals ($\mathbf{y} - \mathbf{D}\mathbf{H}\mathbf{x}^{(s)}$) will not produce an optimal solution, where $\mathbf{x}^{(s)}$ is the estimation value of \mathbf{x} in the s^{th} iteration and it can be obtained by $\mathbf{x}^{(s)} = \Phi\hat{\alpha}$. Here we use an example to investigate the distribution of fitting residuals on image *House*.

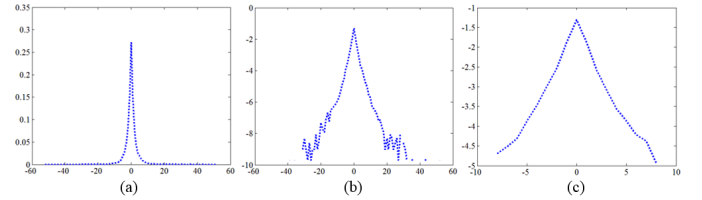


Fig. 1. The distribution of fitting residual in (a) linear and (b) log domain, (c) weighted fitting residual in log domain.

Figure 1(a) and (b) show the distributions of fitting residuals in linear and log domain respectively. As shown in Fig. 1 (b), one can see that the distribution of fitting residuals doesn't follow regular Gaussian distribution and it has a tail. Thus, using the ℓ_2 norm to characterize the data fidelity term is not optimal. In order to weaken the effect of tail, we can modify the fitting residual by assigning a proper weight so that its distribution can be more like Gaussian distribution. Then the ℓ_2 norm can be still used to characterize the data fidelity term. The fitting residuals can be used to guide the setting of weights because tail exists at high residuals. Thus, the weights should be inversely proportional to the fitting residuals. Hereby we give a simple and effective choice of weights \mathbf{w} as:

$$\mathbf{w} = \exp(-c_1(\mathbf{y} - \mathbf{D}\mathbf{H}\mathbf{x}^{(s)}) \odot (\mathbf{y} - \mathbf{D}\mathbf{H}\mathbf{x}^{(s)})). \quad (14)$$

Where c_1 is positive controlling constant and \odot represents component-wise multiplication. Figure 1 (c) shows the distribution of weighted residuals in log domain. We can see that the distribution of weighted residuals is more like Gaussian distribution, which will guarantee that the ℓ_2 norm can be still used in the data fidelity term. Then the model formulated in Eq. (13) can be modified as:

$$\min_{\alpha} \left\{ \left\| \mathbf{W}^{1/2}(\mathbf{y} - \mathbf{D}\mathbf{H}\mathbf{x}) \right\|_2^2 + \gamma \sum_{i=1}^K \left\| \mathbf{R}_i \mathbf{x} - \Phi_i \alpha_i \right\|_2^2 + \sum_{i=1}^K \sum_{j=1}^p \eta_{i,j} (\alpha_{i,j} - \beta_{i,j})^2 \right\} \quad s.t. \quad \mathbf{y} = \mathbf{D}\mathbf{x}. \quad (15)$$

Where $\mathbf{W} = \text{diag}(\mathbf{w})$.

E. Interpolation Algorithm

Given a current estimate of image \mathbf{x} , the weighted encoding matrix \mathbf{W} and the sparse representation α_i can be updated in the next iteration. Then, the updated \mathbf{W} , α_i and dictionary Φ are in turn used to update the estimate of image \mathbf{x} . Such an iteration is stopped until a stopping rule is met.

For a given \mathbf{x} , the Eq. (15) can be rewritten by only retaining the components related to α_i as:

$$\begin{aligned} \hat{\alpha}_i &= \arg \min_{\alpha_i} J(\alpha_i) \\ &= \gamma \left\| \mathbf{R}_i \mathbf{x} - \Phi_i \alpha_i \right\|_2^2 + \sum_{j=1}^p \eta_{i,j} (\alpha_{i,j} - \beta_{i,j})^2 \end{aligned} \quad (16)$$

This is a quadratic problem and we can get a close-form solution by setting $\partial J / \partial \alpha_i = 0$.

$$\alpha_{i,j}^{(s+1)} = \frac{(\Phi_i^T \mathbf{R}_i \mathbf{x}^{(s)})_j + \eta_{i,j} \beta_{i,j} / \gamma}{1 + \eta_{i,j} / \gamma}. \quad (17)$$

After obtaining sparse representations, the image \mathbf{x} can be optimized by minimizing the following function:

$$\begin{aligned} \hat{\mathbf{x}} &= \arg \min_{\mathbf{x}} \left\{ \left\| \mathbf{W}^{1/2}(\mathbf{y} - \mathbf{D}\mathbf{H}\mathbf{x}) \right\|_2^2 + \gamma \sum_{i=1}^K \left\| \mathbf{R}_i \mathbf{x} - \Phi_i \alpha_i \right\|_2^2 \right\} \quad s.t. \quad \mathbf{y} = \mathbf{D}\mathbf{x}. \end{aligned} \quad (18)$$

To solve the above optimization problem, the Augmented Lagrange Multiplier [37], [38] algorithm can be used. The augmented Lagrangian function can be defined as:

$$\begin{aligned} \mathcal{L}(\mathbf{x}, \mathbf{f}, \mu) &= \left\| \mathbf{W}^{1/2}(\mathbf{y} - \mathbf{D}\mathbf{H}\mathbf{x}) \right\|_2^2 + \gamma \sum_{i=1}^K \left\| \mathbf{R}_i \mathbf{x} - \Phi_i \alpha_i \right\|_2^2 \\ &+ \langle \mathbf{f}, \mathbf{y} - \mathbf{D}\mathbf{x} \rangle + \mu \left\| \mathbf{y} - \mathbf{D}\mathbf{x} \right\|_2^2 \end{aligned} \quad (19)$$

We can get the estimate $\mathbf{x}^{(s+1)}$ of image \mathbf{x} in the s^{th} iteration by setting $\partial \mathcal{L} / \partial \mathbf{x} = 0$.

$$\begin{aligned} \mathbf{x}^{(s+1)} &= \left[(\mathbf{D}\mathbf{H})^T \mathbf{W}^{(s)} (\mathbf{D}\mathbf{H}) + \gamma \sum_{i=1}^K \mathbf{R}_i^T \mathbf{R}_i + \mu^{(s)} \mathbf{D}^T \mathbf{D} \right]^{-1} \\ &\left[(\mathbf{D}\mathbf{H})^T \mathbf{W}^{(s)} \mathbf{y} + \gamma \sum_{i=1}^K \mathbf{R}_i^T (\Phi_i \alpha_i) + \mu^{(s)} \mathbf{D}^T \mathbf{y} + \mathbf{D}^T \mathbf{f}^{(s)} / 2 \right] \end{aligned} \quad (20)$$

Where $\mathbf{f}^{(s+1)} = \mathbf{f}^{(s)} + \mu^{(s)} (\mathbf{y} - \mathbf{D}\mathbf{x}^{(s+1)})$ and $\mu^{(s+1)} = t \cdot \mu^{(s)}$ with a constant $t > 1$. Here, the overall interpolation algorithm is summarized in **Algorithm 1**.

Algorithm 1 Weighted Encoding Based Image Interpolation With Nonlocal Linear Regression Model

Input: Low-resolution image \mathbf{y} .

Initialization: Initialize iterator $s = 0$, maximum iteration number T and set:

the initial high-resolution image \mathbf{x} using the Bicubic interpolation method.

the related parameters: $\eta = 1.2, \gamma = 0.1, \mu = 0.68, t = 1.1, m = 15, t = 23$, image block size: 5×5 and $\mathbf{f}^{(0)} = \mathbf{0}$.

PCA sub-dictionaries learned according to the Section II.C

Main Iteration: Increment s by 1 and perform the following steps:

1. Calculate sparse representation $\{\alpha_i\}$ by Eq. (17).

2. Calculate image $\mathbf{x}^{(s+1)}$ by Eq. (20).

3. Update $\mathbf{f}^{(s+1)}$ and $\mu^{(s+1)}$, update weighted matrix $\mathbf{W}^{(s+1)}$ by Eq. (14).

4. Update parameters: $\eta_{i,j} = k_2 / ((\alpha_{i,j}^{(s+1)} - \beta_{i,j})^2 + \varepsilon)$ according to the weight assigned strategy described in [35].

5. Update the adaptive dictionaries $\Phi = [\Phi_1, \Phi_2, \Phi_3, \dots, \Phi_K]$ by Eq. (12).

6. Stopping rule: if $s > T$, stop. Otherwise, do another iteration.

Output: High-resolution image \mathbf{x} .

III. EXPERIMENTAL RESULTS

In all experiments, the size of an image patch is set to 5×5 pixels and the controlling constant c_1 is set to 0.006. Ten benchmark images shown in Fig. 2 are used to evaluate the interpolation performance. These benchmark images are down-sampled firstly. Then low-resolution images are interpolated to generate high-resolution interpolated images that are compared with benchmark images in terms of quantitative measures and visual quality. The PSNR, SSIM [39] and FSIM [40] are used as quantitative evaluation criterions. We compare our proposed method with several state-of-the-art image interpolation methods including: NEDI [4], DFDF [5], and sparse representation based methods including SME [7], SCSR [17] and NARM [19]. All the source codes are downloaded from the homepage of the corresponding authors.

Interpolated *foreman* images with the upscaling factor of 2 are shown in Fig. 3. The Bicubic method generates severe artifacts along edges. Those edge based methods including NEDI and DFDF produce better interpolated results and weaken artifacts, but these methods can't remove artifacts effectively because it is difficult to estimate the edge direction from low-resolution images. The SME and SCSR methods work much better in preserving edges than edge based methods. However, these methods still can't generate sharp edges and the SCSR method produces phantom artifacts along edge. The NARM produces a better interpolated results than above methods and it preserves image edges. However, the learned dictionaries are based on clustering in this method and inappropriate cluster generates spackle noise as shown in Fig. 4. In our method, similar patches are grouped to train adaptive dictionaries instead of clustering, producing a more sparse and accurate representation. This guarantees that our method can produce

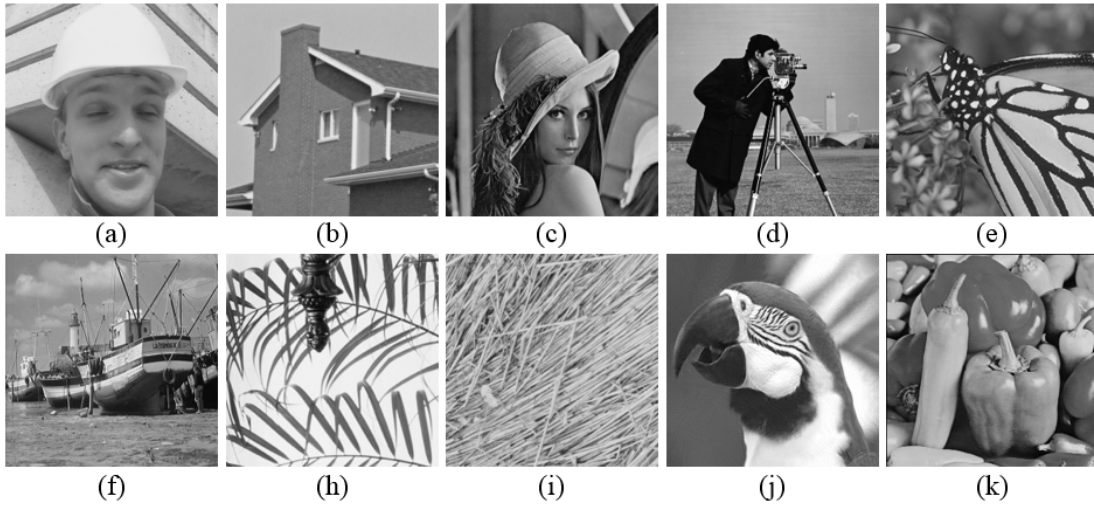


Fig. 2. The ten benchmark images. From left to right and top to bottom: *Foreman*, *House*, *Lena*, *Cameraman*, *Monarch*, *Boat*, *Leaves*, *Straw*, *Parrot* and *Peppers*.

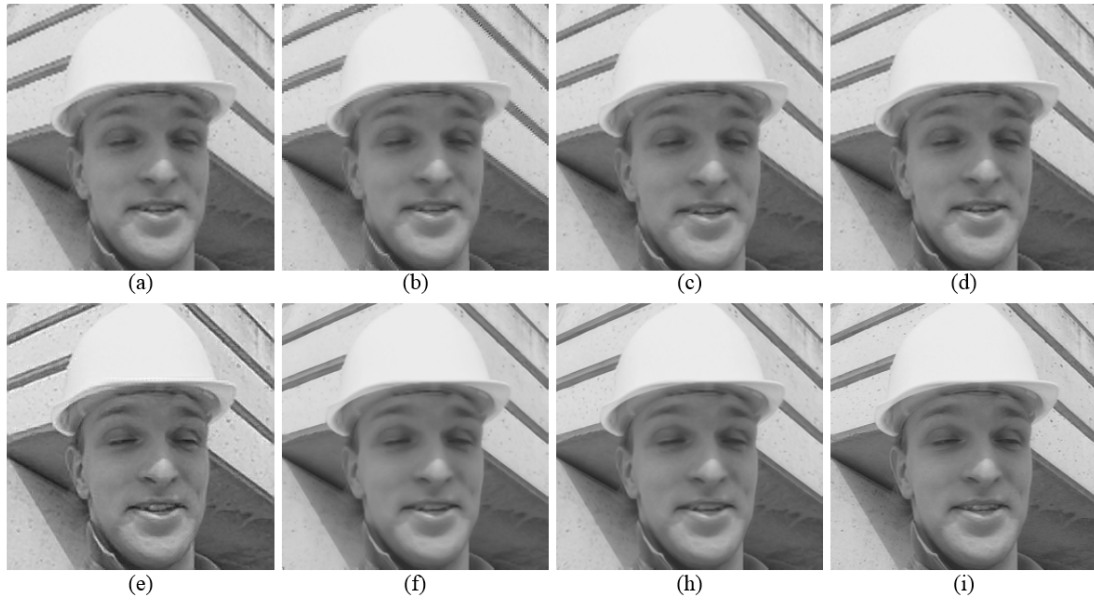


Fig. 3. Interpolated *Foreman* images with upscaling factor of 2. (a) Bicubic (b) NEDI (c) DFDF (d) SME (e) SCSR (f) NARM (g) Ours (h) True image.

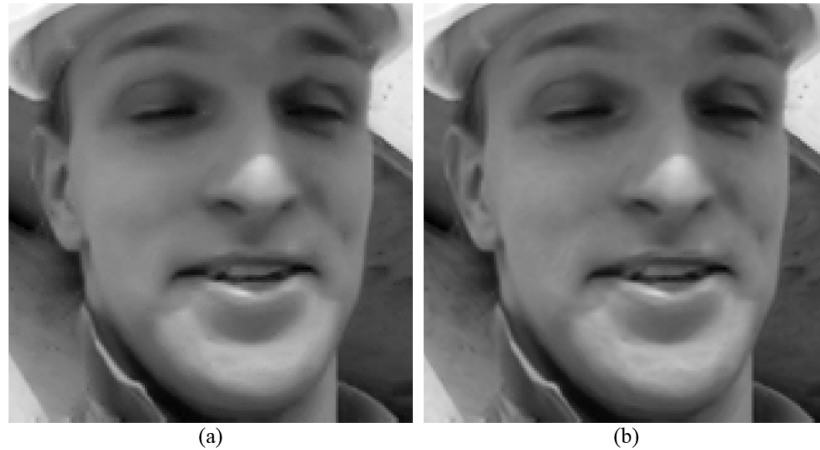


Fig. 4. Comparison of interpolated results. (a) NARM (b) Ours.

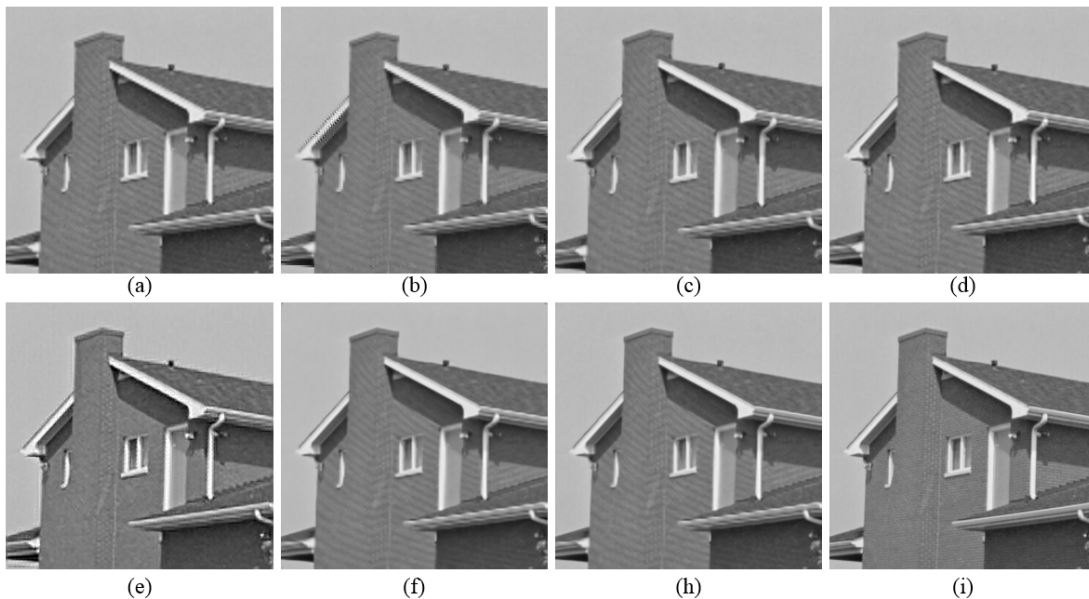


Fig. 5. Interpolated *House* images with upscaling factor of 2. (a) Bicubic (b) NEDI (c) DFDF (d) SME (e) SCSR (f) NARM (h) Ours (I) True image.

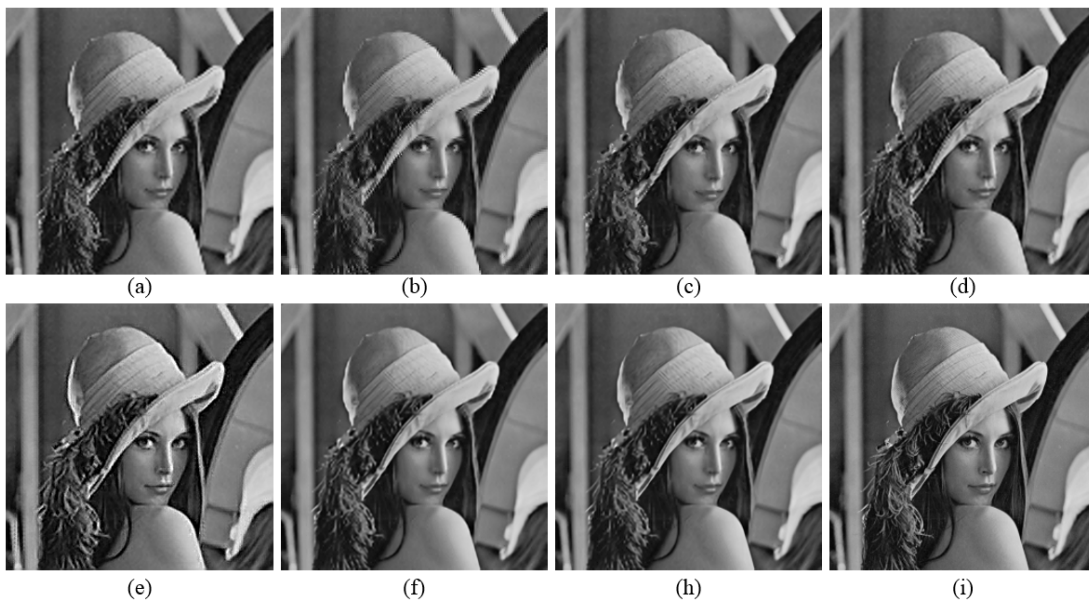


Fig. 6. Interpolated *Lena* images with upscaling factor of 2. (a) Bicubic (b) NEDI (c) DFDF (d) SME (e) SCSR (f) NARM (h) Ours (I) True image.

much better results as shown in Fig. 3(h). For better view spackle noise, the cropped portions of *foreman* image are shown in Fig. 4. One can see that there are severe spackle noise in teeth and ears. Our proposed method produce more clean results while preserving edges. Interpolated *house* and *lena* images with upscaling factor of 2 are shown in Fig. 5 and Fig. 6 respectively. We can see that our proposed method produce much better results than other methods. Our method can reconstruct more clean images while preserving edges such as eaves in Fig. 5 and brims of a hat in Fig. 6.

More interpolated results obtained with upscaling factor of 2 by different methods are list in Table I. The PSNR, SSIM and FSIM results are included in Table I. For each image, from top to bottom are PSNR, SSIM and FSIM values. The

bold number is the best result in each row. We can see that our method achieves higher PSNR, SSIM and FSIM for most benchmark images, which demonstrates that our method is superior to other methods in terms of quantitative measures.

We also conduct experiments with upscaling factor of 3. Since NEDI, DFDF, SME methods are designed for upscaling factor of 2^n , we just compare our proposed method with Bicubic, SCSR and NARM algorithms. The cropped portions of interpolated images with upscaling factor of 3 are shown in Fig. 7 and quantitative measures are list in Table II. For *Leaves* image, we can see that the Bicubic method generates severe artifacts. The SCSR method can weaken artifacts, but it can't generate sharp edges while reconstructing severe phantom. The NARM method is better than the first two methods.

TABLE I
THE PSNR, SSIM, FSIM RESULTS ON TEN TEST IMAGES BY DIFFERENT METHODS WITH UPSCALING FACTOR OF 2.

Image	Bicubic	NEDI	DFDF	SCSR	SME	NARM	Ours
Foreman	35.2710	33.1125	36.6937	32.2409	36.6597	38.3884	38.5234
	0.94661	0.93475	0.95392	0.91756	0.95296	0.95675	0.95709
	0.96411	0.95723	0.97099	0.93464	0.97089	0.97472	0.97681
House	32.2486	30.8612	32.6265	29.1428	33.1718	33.5411	33.6836
	0.88056	0.87772	0.87941	0.86377	0.88415	0.88808	0.88725
	0.93925	0.93168	0.94745	0.89903	0.94978	0.95335	0.95718
Lena	29.3366	28.3854	29.5212	26.8893	30.0699	30.5373	30.6419
	0.90076	0.88702	0.89846	0.86495	0.90840	0.91514	0.91422
	0.95155	0.94223	0.95330	0.91567	0.95674	0.96089	0.96120
Cameraman	25.5058	25.0664	25.7028	24.9155	26.2285	26.0238	26.1372
	0.85946	0.84911	0.86693	0.84639	0.86588	0.87286	0.87091
	0.90165	0.89277	0.91380	0.87300	0.90808	0.91592	0.91790
Monarch	28.4124	26.8815	29.0283	24.8682	29.3786	30.6136	30.7062
	0.93332	0.91324	0.93966	0.86188	0.94480	0.95443	0.95585
	0.93404	0.92397	0.95093	0.85387	0.94267	0.96114	0.96324
Boat	23.8265	23.8807	23.9313	23.4562	24.1617	24.0235	24.1747
	0.75894	0.75954	0.75768	0.76690	0.76966	0.77340	0.77032
	0.89220	0.88846	0.89414	0.86398	0.89581	0.89936	0.90055
Leaves	26.6446	23.6711	27.0701	22.6739	27.8381	29.4344	29.7586
	0.93511	0.88891	0.94297	0.85739	0.94891	0.96559	0.96691
	0.92537	0.89790	0.94687	0.84674	0.94048	0.96437	0.96813
Straw	24.9503	22.8035	24.5504	21.9469	26.2127	27.1254	27.1181
	0.83166	0.76751	0.81380	0.80407	0.87882	0.90318	0.90256
	0.91706	0.88674	0.90933	0.87029	0.93218	0.94247	0.94255
Parrot	29.9697	28.8591	29.8211	27.5569	30.5317	31.3254	31.1769
	0.85128	0.85321	0.85775	0.74726	0.85618	0.87527	0.86273
	0.94709	0.94436	0.94744	0.88352	0.95037	0.95445	0.95308
Peppers	28.3370	24.0673	30.4757	22.5981	29.2094	29.7449	30.1449
	0.91131	0.90219	0.91690	0.85086	0.91690	0.92685	0.92602
	0.94120	0.92159	0.95447	0.93708	0.94644	0.95440	0.95586
Average	28.4503	26.7589	28.9421	25.9183	29.3462	30.0758	30.2066
	0.88090	0.86332	0.88275	0.84983	0.89267	0.90315	0.90138
	0.93135	0.91869	0.93887	0.88945	0.93934	0.94811	0.94964

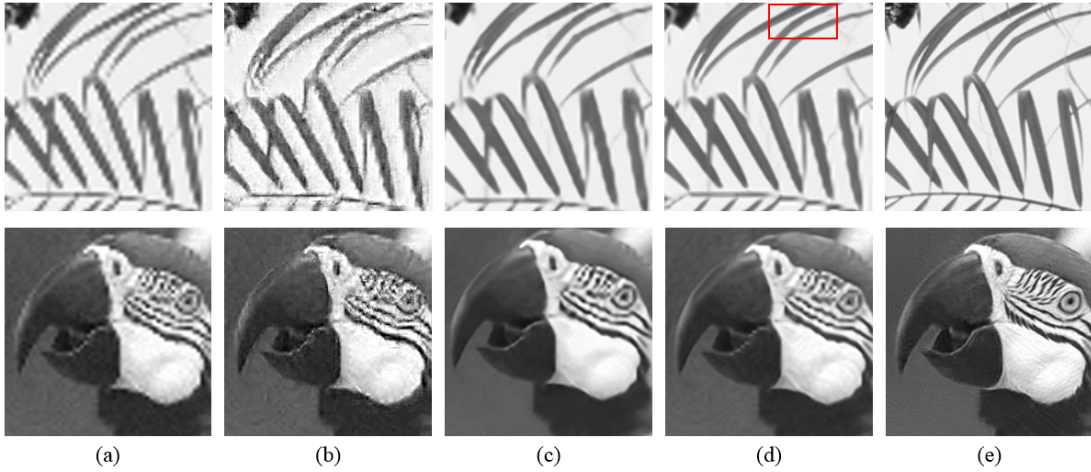


Fig. 7. Interpolated images with upscaling factor of 3. (a) Bicubic (b) SCSR (c) NARM (d) Ours (e) True image.

However, our proposed method preserves edges better such as in the red rectangle region. For *Parrot* image, the NARM produce much smooth results than ours, but it has lower PSNR and FSIM values. According to results list in Table II, one can see that our proposed method achieves higher PSNR, SSIM and FSIM for most benchmark images, which demonstrates that our method is superior to other methods in terms of quantitative measures.

IV. CONCLUSION

In this paper, we propose a novel image interpolation model based on sparse representation. In order to improve interpolation model, we incorporate nonlocal linear regression into it and adopt nonlocal self-similar prior as the regularization term. Besides, we propose a new approach to learn adaptive sub-dictionaries, which ensure that coding coefficients more sparse and accurate. Moreover, we introduce weighted encoding into data fidelity to suppress tailing of fitting residuals. Abundant

TABLE II
THE PSNR, SSIM, FSIM RESULTS ON TEN TEST IMAGES BY DIFFERENT METHODS WITH UPSCALING FACTOR OF 3.

Image	Foreman	House	Lena	Cameraman	Monarch	Boat	Leaves	Straw	Parrot	Peppers	Average
Bicubic	31.8636	28.7770	25.9538	22.5412	24.2393	21.6294	21.7580	21.0395	26.3175	25.2435	24.9363
	0.90333	0.82423	0.81964	0.76651	0.84514	0.62445	0.81254	0.60056	0.79316	0.84831	0.78379
	0.92655	0.87769	0.90303	0.81881	0.85563	0.81557	0.81382	0.81657	0.91292	0.88894	0.86295
SCSR	29.2492	26.6055	23.7016	21.4478	21.8788	20.4430	19.1820	18.8389	24.3585	21.0116	22.6717
	0.85242	0.76605	0.72696	0.70668	0.74839	0.57409	0.70170	0.50466	0.73789	0.73761	0.70565
	0.90159	0.84642	0.85850	0.78663	0.78499	0.79184	0.75651	0.79136	0.88878	0.81078	0.82174
NARM	29.0512	28.4730	26.2937	22.3291	25.2467	21.4987	22.2139	20.9125	26.5037	24.5912	24.7114
	0.91237	0.83704	0.84115	0.77954	0.88830	0.64287	0.87243	0.64142	0.82828	0.86744	0.81108
	0.92570	0.86933	0.90222	0.80844	0.89907	0.80702	0.88036	0.82922	0.90833	0.90075	0.87304
Ours	34.7259	29.7260	26.6696	22.7528	25.8284	21.8178	23.3044	21.3857	27.0098	27.8500	26.1070
	0.92964	0.83699	0.83694	0.78698	0.88628	0.63532	0.87827	0.63047	0.81817	0.87067	0.81097
	0.95048	0.89986	0.91145	0.84395	0.90540	0.81997	0.88954	0.81095	0.92058	0.91832	0.88705

benchmark images are used to evaluate the interpolation performance. Experimental results demonstrate that our proposed method outperforms several state-of-the-art methods in terms of quantitative measures and visual quality.

REFERENCES

- [1] H. S. Hou and H. C. Andrews, "Cubic splines for image interpolation and digital filtering," *IEEE Transactions on Acoustics, Speech, and Signal Processing*, vol. 26, no. 6, pp. 508–517, 1978.
- [2] R. G. Keys, "Cubic convolution interpolation for digital image processing," *IEEE Transactions on Acoustics, Speech, and Signal Processing*, vol. 29, no. 6, pp. 1153–1160, 1981.
- [3] S. Gao and V. Gruev, "Bilinear and bicubic interpolation methods for division of focal plane polarimeters," *Optics Express*, vol. 19, no. 27, pp. 26 161–26 173, 2011.
- [4] X. Li and M. T. Orchard, "New edge-directed interpolation," *IEEE Transactions on Image Processing*, vol. 10, no. 10, pp. 1521–1527, 2001.
- [5] L. Zhang and X. Wu, "An edge guided image interpolation algorithm via directional filtering and data fusion," *IEEE Transactions on Image Processing*, vol. 15, no. 8, pp. 2226–2238, 2006.
- [6] X. Zhang and X. Wu, "Image interpolation by adaptive 2d autoregressive modeling and soft-decision estimation," *IEEE Transactions on Image Processing*, vol. 17, no. 6, pp. 887–896, 2008.
- [7] S. Mallat and G. Yu, "Super-resolution with sparse mixing estimators," *IEEE Transactions on Image Processing*, vol. 19, no. 11, pp. 2889–2900, 2010.
- [8] X. Liu, D. Zhao, R. Xiong, S. Ma, W. Gao, and H. Sun, "Image interpolation via regularized local linear regression," *IEEE Transactions on Image Processing*, vol. 20, no. 12, pp. 3455–3469, 2011.
- [9] S. D. Babacan, R. Molina, and A. K. Katsaggelos, "Total variation super resolution using a variational approach," in *Proc. IEEE International Conference on Image Processing*, San Diego, USA, Oct. 2008, pp. 641–644.
- [10] J. Oliveira, J. M. Bioucas-Dia, and M. Figueiredo, "Adaptive total variation image deblurring: A majorization-minimization approach," *Signal Processing*, vol. 89, no. 9, pp. 1683–1693, 2009.
- [11] M. Lysaker and X. Tai, "Iterative image restoration combining total variation minimization and a second-order functional," *International Journal of Computer Vision*, vol. 66, no. 1, pp. 5–18, 2006.
- [12] A. Beck and M. Teboulle, "Fast gradient-based algorithms for constrained total variation image denoising and deblurring problems," *IEEE Transactions on Image Processing*, vol. 18, no. 11, pp. 2419–2434, 2009.
- [13] B. Yang and S. Li, "Multifocus image fusion and restoration with sparse representation," *IEEE Transactions on Instrumentation and Measurement*, vol. 59, no. 4, pp. 884–892, 2009.
- [14] M. Elad and M. Aharon, "Image denoising via sparse and redundant representations over learned dictionaries," *IEEE Transactions on Image Processing*, vol. 15, no. 12, pp. 3736–3745, 2006.
- [15] M. Aharon, M. Elad, and A. Bruckstein, "K -svd: An algorithm for designing overcomplete dictionaries for sparse representation," *IEEE Transactions on Signal Processing*, vol. 54, no. 11, pp. 4311–4322, 2006.
- [16] J. Mairal, M. Elad, and G. Sapiro, "Sparse representation for color image restoration," *IEEE Transactions on Image Processing*, vol. 17, no. 1, pp. 53–69, 2008.
- [17] J. Yang, J. Wright, T. Huang, and Y. Ma, "Image super-resolution via sparse representation," *IEEE Transactions on Image Processing*, vol. 19, no. 11, pp. 2861–2873, 2010.
- [18] W. Dong, L. Zhang, G. Shi, and X. Wu, "Image deblurring and super-resolution by adaptive sparse domain selection and adaptive regularization," *IEEE Transactions on Image Processing*, vol. 20, no. 7, pp. 1838–1857, 2011.
- [19] W. Dong, L. Zhang, R. Lukac, and G. Shi, "Sparse representation based image interpolation with nonlocal autoregressive modeling," *IEEE Transactions on Image Processing*, vol. 22, no. 4, pp. 1382–1394, 2013.
- [20] W. Dong, L. Zhang, G. Shi, and X. Li, "Nonlocally centralized sparse representation for image restoration," *IEEE Transactions on Image Processing*, vol. 22, no. 4, pp. 1620–1630, 2013.
- [21] J. Jiang, L. Zhang, and J. Yang, "Mixed noise removal by weighted encoding with sparse nonlocal regularization," *IEEE Transactions on Image Processing*, vol. 23, no. 6, pp. 2651–2662, 2014.
- [22] J. Liu, X. Tai, H. Huang, and Z. Huan, "A weighted dictionary learning models for denoising images corrupted by mixed noise," *IEEE Transactions on Image Processing*, vol. 22, no. 3, pp. 1108–1120, 2013.
- [23] Y. Romano, M. Protter, and M. Elad, "Single image interpolation via adaptive nonlocal sparsity-based modeling," *IEEE Transactions on Image Processing*, vol. 23, no. 7, pp. 3085–3098, 2014.
- [24] H. Liu and S. Li, "Target detection using sparse representation with element and construction combination feature," *IEEE Transactions on Instrumentation and Measurement*, vol. 64, no. 2, pp. 290–298, 2014.
- [25] L. Fang and S. Li, "Face recognition by exploiting local gabor features with multitask adaptive sparse representation," *IEEE Transactions on Instrumentation and Measurement*, vol. 64, no. 10, pp. 2605–2615, 2015.
- [26] L. Fang, C. Wang, S. Li, and J. A. Benediktsson, "Hyperspectral image classification via multiple-feature-based adaptive sparse representation," *IEEE Transactions on Instrumentation and Measurement*, vol. 66, no. 7, pp. 1646–1657, 2017.
- [27] C. Dong, C. Loy, K. He, and X. Tang, "Image super-resolution using deep convolutional networks," *IEEE Transactions on Pattern Analysis and Machine Intelligence*, vol. 38, no. 2, pp. 295–307, 2014.
- [28] W. Shi, J. Caballero, F. Huszar, J. Totz, A. P. Aitken, R. Bishop, D. Rueckert, and Z. Wang, "Real-time single image and video super-resolution using an efficient sub-pixel convolutional neural network," in *Proc. IEEE International Conference on Computer Vision and Pattern Recognition (CVPR)*, 2016, pp. 1874–1883.
- [29] J. Kim, J. K. Lee, and K. M. Lee, "Deeply-recursive convolutional network for image super-resolution," in *Proc. IEEE International Conference on Computer Vision and Pattern Recognition (CVPR)*, 2016.
- [30] Y. Tai, J. Yang, and X. Liu, "Image super-resolution via deep recursive residual network," in *Proc. IEEE International Conference on Computer Vision and Pattern Recognition (CVPR)*, 2017.
- [31] E. J. Candes, "Compressive sampling," in *Proc. International Congress of Mathematicians*, 2006, pp. 1433–1452.
- [32] J. A. Tropp and S. J. Wright, "Computational methods for sparse solution of linear inverse problems," in *Proc. IEEE*, 2010, pp. 948–958.
- [33] A. Buades, B. Coll, and J. M. Morel, "A non-local algorithm for image denoising," in *Proc. IEEE International Conference on Computer Vision and Pattern Recognition (CVPR)*, 2005, pp. 60–65.
- [34] K. Dabov, A. Foi, V. Katkovnik, and K. Egiazarian, "Image denoising by sparse 3-d transform-domain collaborative filtering," *IEEE Transactions on Image Processing*, vol. 16, no. 8, pp. 2080–2095, 2007.

- [35] L. Zhang, W. Dong, D. Zhang, and G. Shi, "Two-stage image denoising by principal component analysis with local pixel grouping," *Pattern Recognition*, vol. 43, pp. 1531–1549, 2010.
- [36] R. Chartrand and W. Yin, "Iteratively reweighted algorithms for compressive sensing," in *Proc. IEEE International Conference on Acoustics, Speech and Signal Processing*, 2008, pp. 3869–3872.
- [37] D. Bertsekas, *Constrained Optimization and Lagrange Multiplier Method*. Belmont Massachusetts: Athena Scientific, 1996.
- [38] —, *Nonlinear Programming*. Belmont Massachusetts: Athena Scientific, 1999.
- [39] Z. Wang, A. C. Bovik, H. R. Sheikh, and E. P. Simoncelli, "Image quality assessment: from error measurement to structural similarity," *IEEE Transactions on Image Processing*, vol. 3, no. 4, pp. 600–612, 2004.
- [40] L. Zhang, L. Zhang, X. Mou, and D. Zhang, "Fsim: A feature similarity index for image quality assessment," *IEEE Transactions on Image Processing*, vol. 20, no. 8, pp. 2378–2386, 2011.



Junchao Zhang received the B.S. degree in mechanical engineering and automation from HoHai University in 2014 and Ph. D. degree in pattern recognition and intelligent systems from Shenyang Institute of Automation, Chinese Academy of Sciences in 2019. From 2017 to 2018, he visited the University of Arizona as a joint Ph. D. student. Now he works at School of Aeronautics and Astronautics, Central South University. His research interests include polarization imaging, image processing, image measurement, machine learning and pattern recognition.